Supplementary information

Dissolution of Ti porous transport layer in proton exchange membrane water electrolyzer

Junsic Cho,[a,‡] Dong Hyun Kim,[a,‡] Min Wook Noh,[a] Haesol Kim,[a] Hong-Gyun Oh,[b] Pilyoung Lee,[c] Soobin Yoon,[c] Wangyun Won[d], Young-June Park,[c*] Ung Lee[e,f,g*] and Chang Hyuck Choi[a,h*]

[a]Department of Chemistry, Pohang University of Science and Technology (POSTECH), Pohang 37673, Republic of Korea

[b]Global Sales Department, Shinsung C&T, Suwon 16648, Republic of Korea

[c]Hydrogen and Fuel Cell Development Center, Hyundai Motor Group, Yongin 16891, Republic of Korea

[d]Department of Chemical and Biological Engineering, Korea University, 145, Seoul 02841, Republic of Korea

[e]Clean Energy Research Center, Korea Institute of Science and Technology, Seoul 02792, Republic of Korea

[f]Green School, Korea University, 145 Anam-ro, Seongbuk-gu, Seoul 02841, Republic of Korea

[g]KIST Europe, Korea Institute of Science and Technology Europe, Campus E71, Saarbrücken 66123, Germany

[h]Institute for Convergence Research and Education in Advanced Technology (I-CREATE), Yonsei University, Seoul 03722, Republic of Korea

[‡]These authors contributed equally to this work.

[*]Corresponding authors: (Y.J.P) yjpark2935@hyundai.com; (U.L) ulee@kist.re.kr; (C.H.C) chchoi@postech.ac.kr

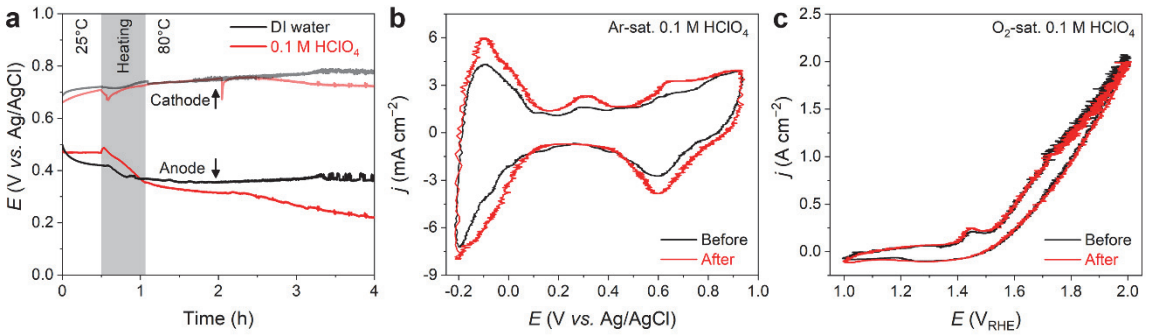

Fig. S1 (a) OCP values of Ti PTL anode and Pd/C GDE cathode with a supply of O_2-saturated DI water and 0.1 M $HClO_4$. (b) CV responses of Pt-coated Ti PTL before and after Protocols 1–4 with a supply of Ar-saturated 0.1 M $HClO_4$ at 80 °C. (c) CV responses of IrO_2 anode with Pt/C cathode (anode: 4 $mg_{cat.}$ cm^{-2} of IrO_2, cathode: 0.5 mg_{Pt} cm^{-2} of Pt/C) before and after Protocols 1–4 with a supply of O_2-saturated 0.1 M $HClO_4$ at 80 °C. Protocols 1–4 are consecutive operations of chronoamperometry, cyclic voltammetry, pulsed potentiometry, and OCP with lower and upper potential limits of 1 and 2 V_{RHE} (see detailed in the main manuscript).

Additional note: To examine the stability of our experimental setup, we first measured the OCP of each Ti PTL anode and Pd/C GDE cathode with a supply of O_2-saturated DI water or 0.1 M $HClO_4$ (Fig. S1a). The results show stable OCP values for both the anode and cathode during 4 h operation with the supply of DI water. On the other hand, with the supply of 0.1 M $HClO_4$ electrolyte, the OCP values were not stable and exhibited considerable changes. However, the inconsistent OCP values do not conclusively imply instability in our setup equipped with the reference electrode, but possibly originate from simultaneous modifications of the less noble electrode surface under exposure to acidic media, as shown in this work (*i.e.*, considerable Ti dissolution and Ti oxide formation). Therefore, we employed Pt-coated Ti PTL as both anode and cathode and measured their CVs before and after Protocols 1–4 — consecutive operations of chronoamperometry, CV, pulsed potentiometry, and OCP with lower and upper potential limits of 1 and 2 V_{RHE} (see details in the main manuscript) — with a supply of Ar-saturated 0.1 M $HClO_4$ electrolyte (Fig. S1b). The voltammograms revealed no considerable potential shift in the hydrogen underpotential deposition (H_{UPD}) and Pt reduction/oxidation regions, *i.e.*, the fingerprint of Pt, before and after the operation. Indeed, when we employed IrO_2 as the anode, its polarization curves completely collapsed before and after Protocols 1–4 (Fig. S1c), clearly confirming the validity of our experimental setup, at least during our experimental timescale.

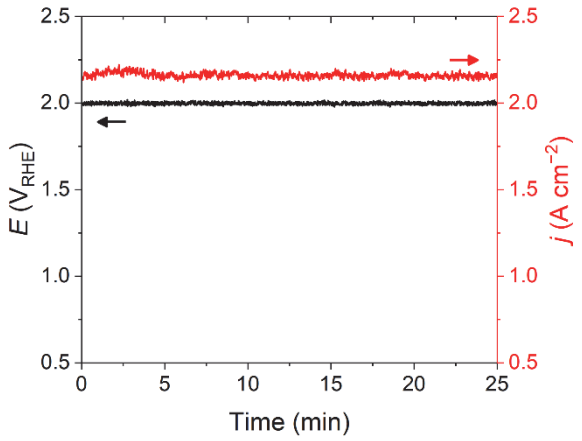

Fig. S2 Current-time response of our homemade PEMWE at an anode potential of 2 V_{RHE} and a cell temperature of 80 °C. In this experiment, a 0.36 cm^2 commercial MEA with anode IrO_2 (4 $mg_{cat.}$ cm^{-2}) and cathode Pt/C (0.5 mg_{Pt} cm^{-2}) catalysts was used. DI water flowed into both the anode and cathode sides at a flow rate of 5 mL min^{-1}.

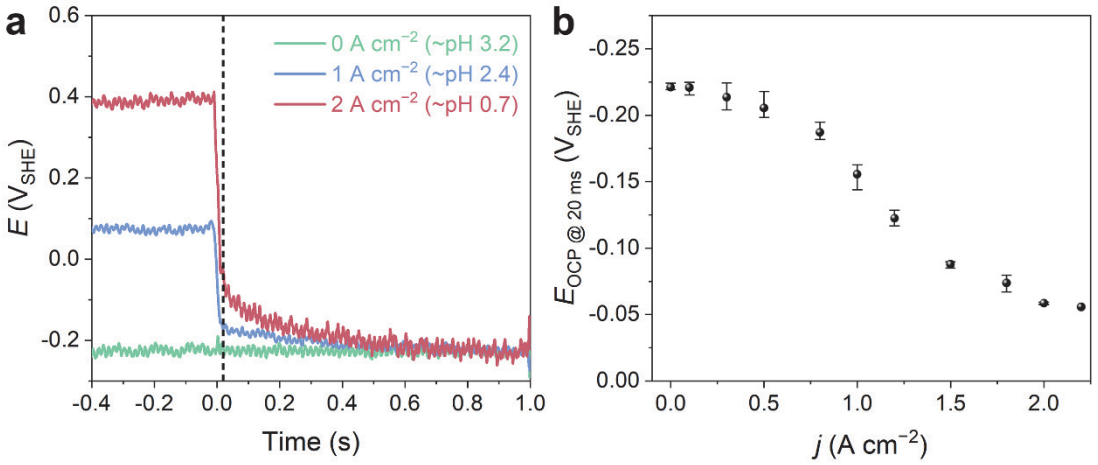

Fig. S3 (a) OCP decay transient after applying 0, 1, and 2 A cm^{-2}. (b) Correlation between *j* and OCP values collected at 20 ms after the potential transient to OCP.

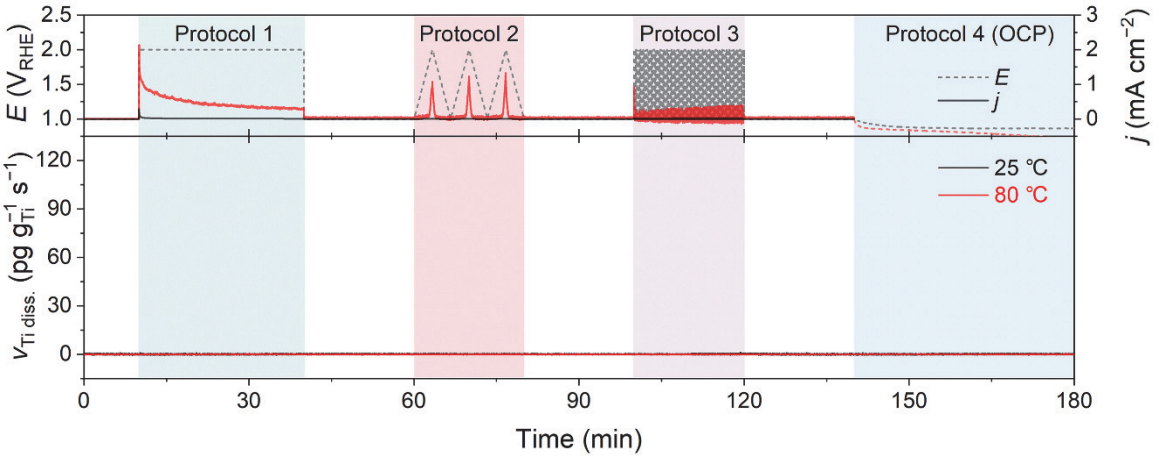

Fig. S4 Real-time dissolution profiles of Ti PTL measured in the order of Protocols 1 → 2 → 3 with a supply of O_2-saturated DI water at 25 and 80 °C.

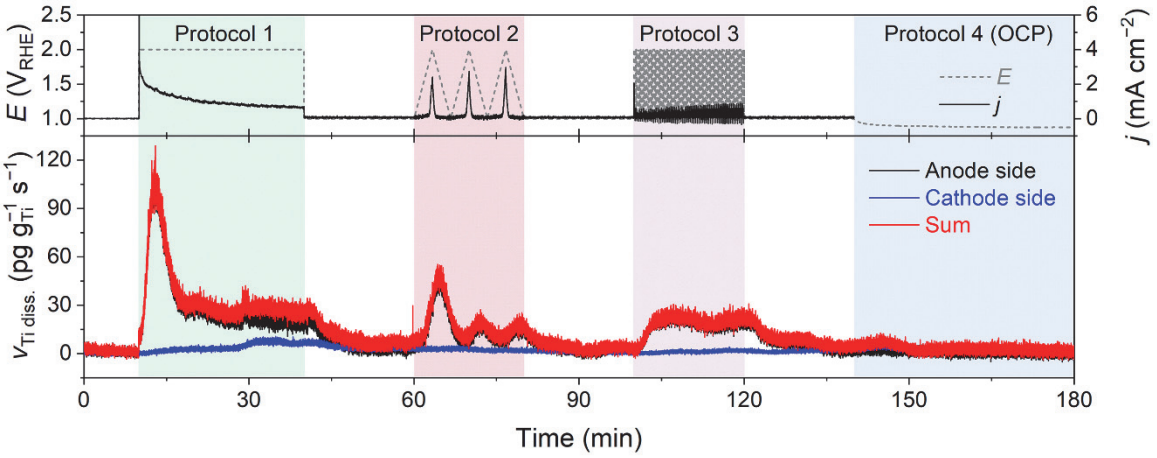

Fig. S5 Real-time Ti dissolution of Ti PTL measured at the end of anolyte and catholyte, respectively.

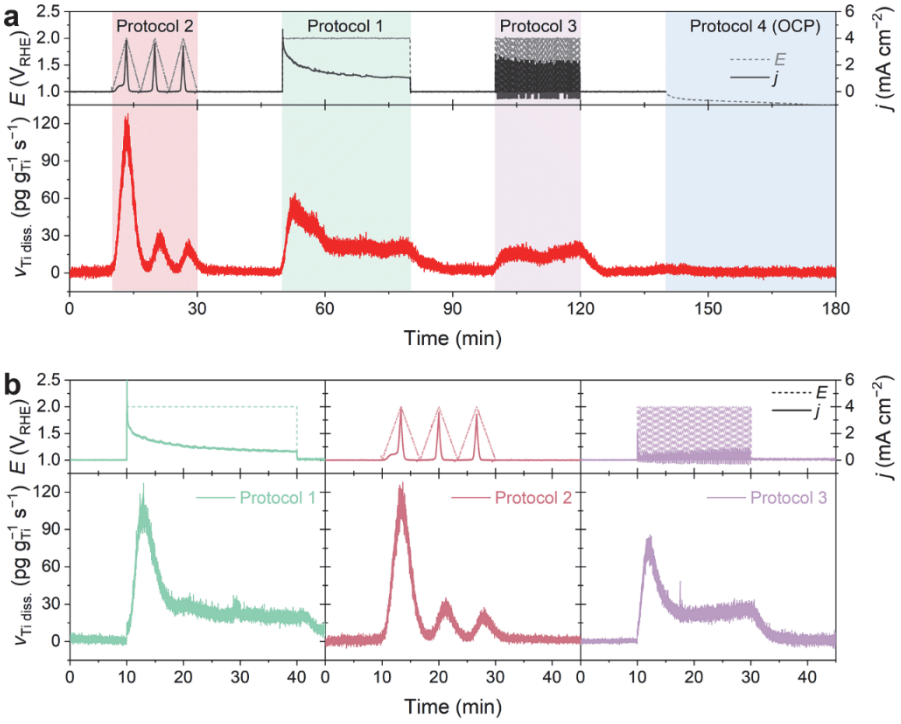

Fig. S6 (a) Real-time dissolution profiles of Ti PTL measured in the order of Protocols 2 → 1 → 3 at 80 °C with a supply of O_2-saturated 0.1 M $HClO_4$ feedstock. (b) For comparison, the Ti dissolution profiles for each protocol, when performed first on a fresh sample, are shown.

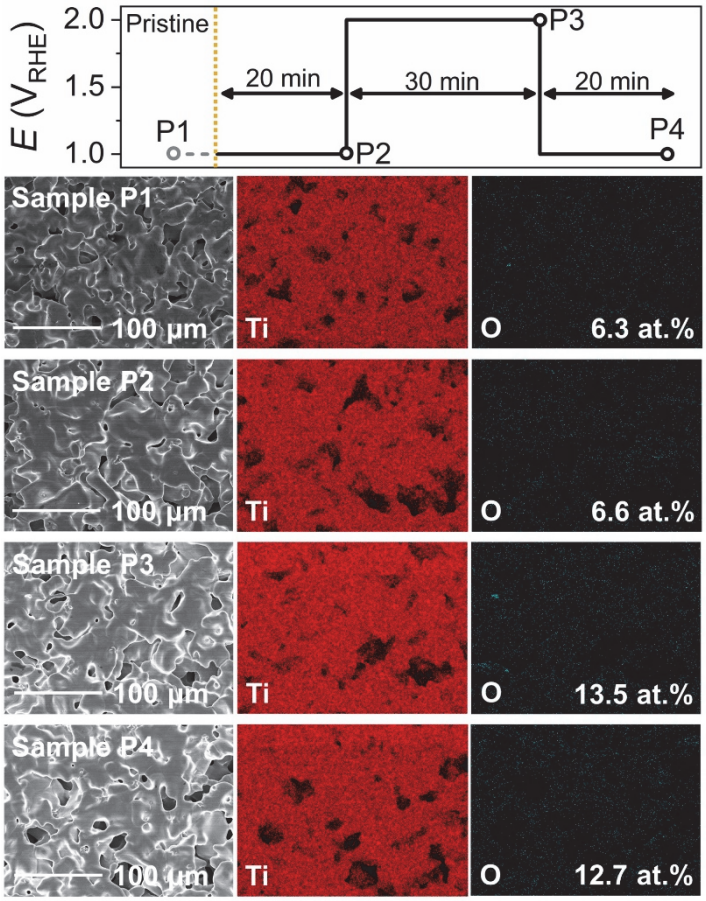

Fig. S7 SEM and EDS results of Ti PTL before and after its polarization in O_2-saturated 0.1 M $HClO_4$ at 25 °C. Sample P1 is a pristine Ti PTL. Samples P2, P3, and P4 are Ti PTLs colleted after its polarization at a certain operating point, which is indicated in the upper panel.

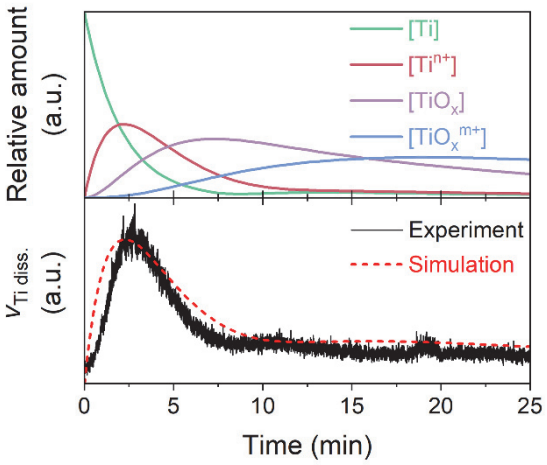

Fig. S8 Computational modeling of Ti PTL dissolution during a potential hold at 2 V_{RHE} at 80 °C (see details of computational modeling in the additional note below).

Additional note

The simplified reaction steps involved in the dissolution of Ti PTL during a potential jump from 1 to 2 V_{RHE} and subsequent potential hold at 2 V_{RHE} are given below:

$Ti \rightarrow Ti^{n+} + ne^-$ (1) with k_1

$Ti^{n+} \rightarrow Ti^{n+}_{Bulk}$ (2) with k_2

$Ti^{n+} + xH_2O \rightarrow TiO_x + xH_2$ (3) with k_3

$TiO_x \rightarrow TiO_x^{m+} + me^-$ (4) with k_4

$TiO_x^{m+} \rightarrow TiO_x^{m+}{}_{Bulk}$ (5) with k_5

The process initiates with the electrochemical oxidative dissolution of metallic Ti to form Ti^{n+} (Eqn. 1), followed by its diffusion from the interface to the bulk feedstock (Eqn. 2). A portion of Ti^{n+} undergoes hydrolysis and precipitates onto the PTL, forming a TiO_x passivation layer (Eqn. 3). Under highly anodic polarization, TiO_x is further dissolved electrochemically (Eqn. 4), and it subsequently diffuses to the bulk feedstock (Eqn. 5) before being monitored by online ICP-MS.

We used a computational modeling approach to predict the dynamic behavior of Ti dissolution, which is governed by a set of ordinary differential equations (ODEs). These equations describe the temporal evolution of four key variables, representing the concentrations of different substances in a reaction pathway. The model structure is defined by the differential equations (Eqns. 6–9). Note that, since the reaction occurs under potentiostatic conditions, we can set the rate constants of steps 1 and 4 as k_1 and k_4, respectively, rather than using formal expressions considering the charge transfer coefficient and biased potential.

$$\frac{d[\mathrm{Ti}]}{dt} = -k_1[\mathrm{Ti}] \quad (6)$$

$$\frac{d[\mathrm{Ti^{n+}}]}{dt} = k_1[\mathrm{Ti}] - k_2[\mathrm{Ti^{n+}}] - k_3[\mathrm{Ti^{n+}}] \quad (7)$$

$$\frac{d[\mathrm{TiO_x}]}{dt} = k_3[\mathrm{Ti^{n+}}] - k_4[\mathrm{TiO_x}] \quad (8)$$

$$\frac{d[\mathrm{TiO_x^{m+}}]}{dt} = k_4[\mathrm{TiO_x}] - k_5[\mathrm{TiO_x^{m+}}] \quad (9)$$

A conditional mechanism has been introduced into the ODE solver, where $[\mathrm{Ti}]$ increases by the same amount as $[\mathrm{TiO_x}]$ decreases, modeling a compensatory effect coverage of metallic Ti. However, increases in $[\mathrm{TiO_x}]$ do not affect $[\mathrm{Ti}]$, which further improves the accuracy of the model in reflecting the dissolution process. We set initial value of [TiO_x] to zero. The total Ti dissolution rate measured by online ICP-MS can be expressed as:

$$\frac{d[\mathrm{Ti^{n+}_{Bulk}}]}{dt} + \frac{d[\mathrm{Ti^{m+}_{Bulk}}]}{dt} = k_2[\mathrm{Ti}^{n+}] + k_5[\mathrm{Ti}^{m+}] \quad (10)$$

To solve these ODEs and explore the system behavior under various conditions, we utilized MATLAB ode45 solver, a versatile tool for dealing with stiff and non-stiff differential equation systems. The adaptive time-stepping algorithm of the solver ensures accurate results over a wide range of parameter values. We also used a genetic algorithm (GA) for parameter optimization to fit our model to experimental data. This optimization process involved defining a cost function based on the sum of the squared differences between the model predictions and the experimental observations, which the GA minimized by adjusting the kinetic parameters and the optimum kinetic parameters were identified as k_1 = 0.0081, k_2 = 0.0032, k_3 = 0.0037, k_4 = 0.0015, and k_5 = 0.001. The results imply that the electrochemical oxidative dissolution of metallic Ti has a faster rate than both diffusion and Ti oxidation, resulting in a gradual decrease in metallic Ti concentration that vanishes after 10 minutes. In contrast, the dissolution rate of TiO_x, k_4, is significantly slower than its formation rate. Consequently, this difference allows TiO_x to maintain a comparatively high concentration throughout the dissolution reaction.

However, it is important to note that while the above simple reactions greatly simulate our experimental results (Fig. 3c), more complex reactions and elaborated modeling processes may be necessary for a comprehensive understanding of entire Ti dissolution reactions. Nonetheless, with this simplified modeling approach, we can envision that:

1) A rapid oxidation of metallic Ti to Ti^{n+} and its subsequent diffusion to the bulk feedstock mainly corresponds to initially intensive Ti dissolution once the potential jumps from 1 to 2 V_{RHE}.

2) The subsequent exponential decay of Ti dissolution rate with marginal but consistent Ti dissolution after 500 s corresponds to the formation of the TiO_x passivation layer and its slow dissolution, respectively.

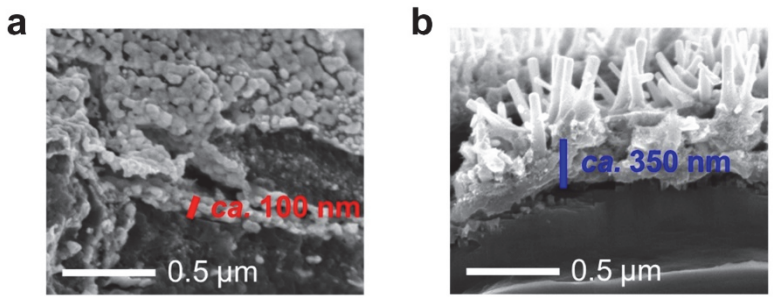

Fig. S9 Cross-sectional SEM images of (a) Pt- and (b) IrO_2-coated Ti PTLs.

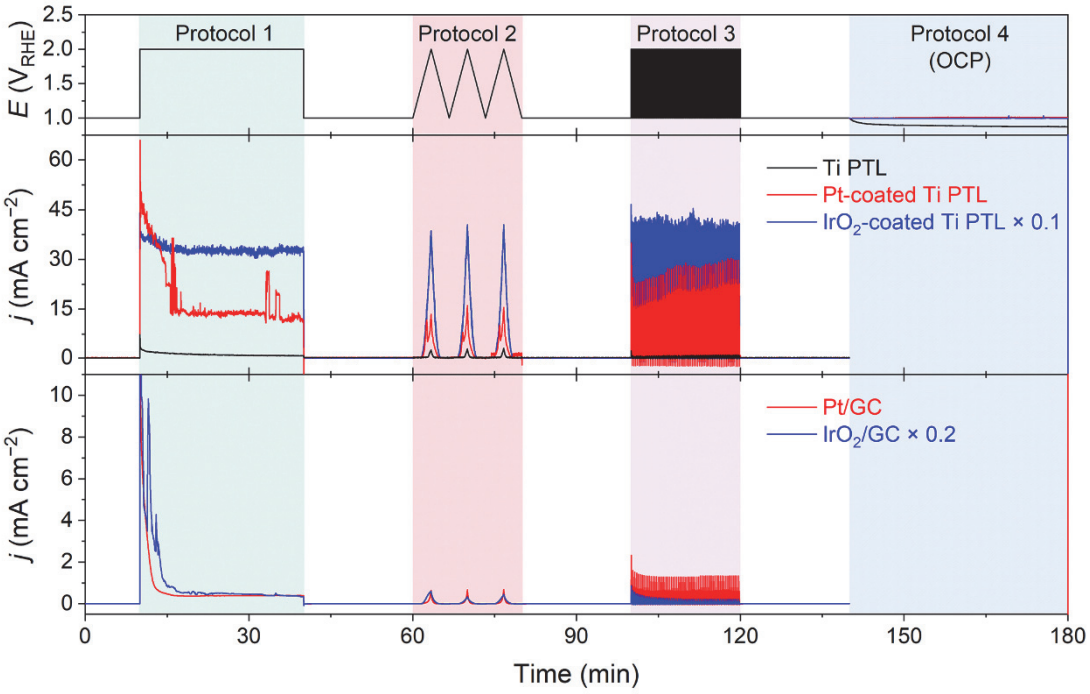

Fig. S10 Current densities of Ti PTL, modified Ti PTLs, and commercially available Pt and IrO_2 nanoparticles deposited on a GC electrode during Protocol 1–4 with a supply of O_2-saturated 0.1 M $HClO_4$ feedstock. The results correspond to the online ICP-MS results in Fig. 4c and Fig. 5.

Table S1. Pt and Ir contents on the modified Ti PTLs.

Sample	Pt (mg cm^{-2})	Ir (mg cm^{-2})
Pt-coated Ti PTL	1.68	
IrO_2-coated Ti PTL		0.36